Design of the Pacific DC Intertie Wide Area Damping Controller

Brian J. Pierre, *Member, IEEE*, Felipe Wilches-Bernal, *Member, IEEE*, David A. Schoenwald, *Senior Member, IEEE*, Ryan T. Elliott, *Member, IEEE*, Daniel J. Trudnowski, *Fellow, IEEE*, Raymond H. Byrne, *Fellow, IEEE*, and Jason C. Neely, *Senior Member, IEEE*

***Abstract*—This paper describes the design and implementation of a proof-of-concept Pacific dc Intertie (PDCI) wide area damping controller and includes system test results on the North American Western Interconnection (WI). To damp inter-area oscillations, the controller modulates the power transfer of the PDCI, a ±500 kV dc transmission line in the WI. The control system utilizes real-time phasor measurement unit (PMU) feedback to construct a commanded power signal which is added to the scheduled power flow for the PDCI. After years of design, simulations, and development, this controller has been implemented in hardware and successfully tested in both open and closed-loop operation. The most important design specifications were safe, reliable performance, no degradation of any system modes in any circumstances, and improve damping to the controllable modes in the WI. The main finding is that the controller adds significant damping to the modes of the WI and does not adversely affect the system response in any of the test cases. The primary contribution of this paper, to the state of the art research, is the design methods and test results of the first North American real-time control system that uses wide area PMU feedback.**

***Index Terms*—HVDC transmission control, damping control, phasor measurement unit, power system dynamic stability, control systems, real time systems, small signal stability, wide area networks, oscillations, HVDC, high voltage DC, PMU, WECC, delay, wide area control, modal analysis, real-time control, western interconnection.**

I. Introduction

LARGE power systems with generation and load separated by long transmission corridors are prone to inter-area oscillations. The North American Western Interconnection (WI) has multiple inter-area modes of oscillation that have been thoroughly characterized [1]. Previous low damping events [2] and increased power system congestion has prompted new engineering developments to improve damping of these system modes. Recent research activities have utilized wide area measurement system technologies such as phasor measurement units (PMUs) in real-time control to improve damping of inter-area oscillations [3], [4].

The damping controller (DCON) utilizes a control scheme to damp inter-area oscillations by modulating the power on the Pacific dc Intertie (PDCI), an 846 mile long ±500 kV dc transmission line in the North American Western Interconnection (WI) with a capacity of 3,220 MW. The control system utilizes real-time PMU feedback to construct a supplemental commanded power signal for the PDCI. The DCON modulates the active power flow on the PDCI by up to ±125 MW based on the frequency difference between two areas.

The implemented controller focuses on damping the North-South B mode of oscillation in the WI which is typically near 0.4 Hz. The WI modes have been significantly studied over decades [1], [5], and are depicted in Fig. 1. The North-South B mode has been shown to be problematic in the past, including a wide area blackout in 1996 that in part resulted from an under damped condition of the North–South B mode [2]. This blackout affected the entire North American west coast and cost utilities over a billion dollars and cost society much more. To maintain higher damping levels, utilities have decreased the power transfer capacity of the California-Oregon Intertie (COI) corridor. The motivation of this project is to increase the damping of the North–South B mode, therefore reducing the chance of large scale blackouts, and in the long run allowing increased capacity of the COI corridor, which has a large financial incentive. An equally important part of this project is safe, robust, reliable performance, no degradation of any system aspects in any cases. For further information on the supervisory system, which enables the DCON to maintain robust reliable performance, the interested reader is referred to [6].

The first experiments related to this idea date back to the 1970s [7]. In those experiments the PDCI power flow was modulated using local feedback. These tests were successful in the fact that they improved damping of the desired mode, but they destabilized a different mode [1]. The change which has made this project successful is the large-scale installation of PMUs

Manuscript received July 13, 2018; revised December 19, 2018; accepted March 1, 2019. Date of publication March 8, 2019; date of current version August 22, 2019. This work was supported in part by the Bonneville Power Administration Technology Innovation Office (TIP 289) and the U.S. DOE Office of Electricity Transmission Reliability and Energy Storage Programs. Sandia National Laboratories is a multimission laboratory managed and operated by National Technology and Engineering Solutions of Sandia, LLC, a wholly owned subsidiary of Honeywell International, Inc., for the U.S. Department of Energy's National Nuclear Security Administration under contract DE-NA0003525. The views expressed in the article do not necessarily represent the views of the U.S. Department of Energy or the United States Government SAND2019-3169J. Paper no. TPWRS-01084-2018. *(Corresponding author: Brian J. Pierre.)*

B. Pierre, F. Wilches-Bernal, D. Schoenwald, R. Elliott, R. Byrne, and J. Neely are with the Sandia National Laboratories, Albuquerque, NM USA (e-mail: bjpierr@sandia.gov; fwilche@sandia.gov; daschoe@sandia.gov; ryanelliott@ieee.org; rhbyrne@sandia.gov; jneely@sandia.gov).

D. Trudnowski is with the Montana Technological University, Butte, MT USA (e-mail: dtrudnowski@mtech.edu).

Color versions of one or more of the figures in this paper are available online at http://ieeexplore.ieee.org.

Digital Object Identifier 10.1109/TPWRS.2019.2903782

Fig. 1. Modes of oscillation in the North American Western Interconnection. The typical modal frequencies are: North-South B ∼0.4 Hz, North-South A ∼0.25 Hz, Montana-NW ∼0.8 Hz, East-West ∼0.5 Hz, and BC-US ∼0.6 Hz.

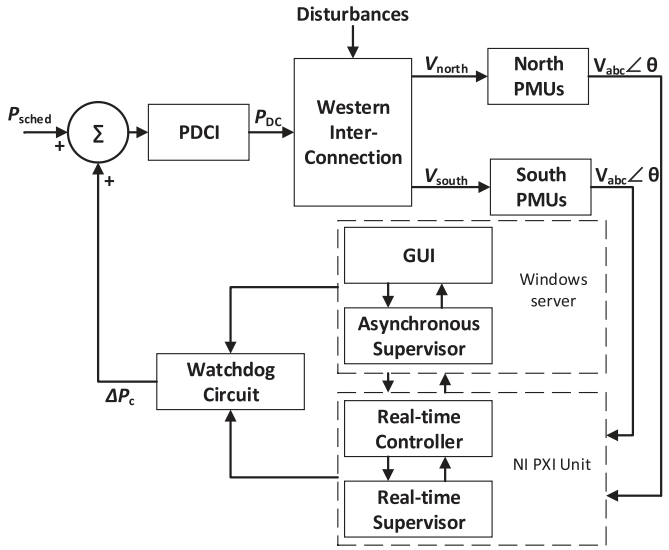

Fig. 2. The DCON overall architecture.

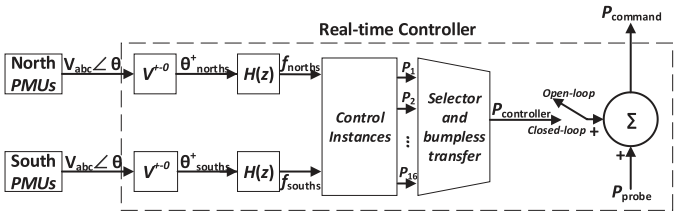

Fig. 3. The real-time controller block diagram from Fig. 2.

across the WI. The control strategy in this project uses wide area measurement feedback. It should also be noted that the system has significantly expanded since the 1970s experiments in [7] including the interconnection of Alberta, Canada.

Significant research has investigated the use of real-time wide area measurements to improve power system stability. In Norway, a project was completed in which the output of a static VAr compensator is modulated using PMUs in real-time control to improve damping of inter-area oscillations [4]. In addition, a project in southern China utilized HVDC modulation to improve damping of inter-area modes [3].

The primary contributions of this paper are as follows:

1) The design and implementation of the first wide area control system in North America that uses real-time PMU feedback.
2) System test results of a control system which damps inter-area oscillations in the WI.
3) Simulation results indicating significant damping improvement during severe contingencies.
4) The compensation design that is utilized, and considerations for designing a real-time control system using PMU feedback.
5) Methods to account for abnormal data conditions: data arrival time inconsistencies, data drop outs, data delays, and asymmetries in feedback signal delays.

The remainder of this paper is organized as follows: the control strategy is further described in the Section II, Section III explains the filter design, Section IV discusses the layout of the software code, Section V discusses the impact of delays, data inconsistences, and time alignment of feedback signals, Section VI presents the system test results and how they compare to simulation, and Section VII provides conclusions and discusses future work.

II. Control Strategy

The damping controller discussed in this paper modulates the power flow on the PDCI using feedback from wide area PMU measurements. Real power is symmetrically injected into the AC system at the two ends of the HVDC line proportional to the difference in frequency between two points of measurement [1]. To compute the frequency difference, voltage phasors are measured in the north and south as depicted in Fig. 1. The positive sequence phasors are then passed through a custom numerical differentiator, $H(z)$. After time-aligning the signals, the difference between the two measurements, Δf, is computed. The frequency difference is then passed through a gain function, K, to obtain the power modulation command, $P_{\mathrm{controller}}$, in MW

$$\Delta f = f_n\left(t-\tau\right) - f_s\left(t-\tau\right), \tag{1}$$

$$P_{\mathrm{controller}} = K(\Delta f). \tag{2}$$

The block diagram in Fig. 2 depicts the overall control architecture. There are three key components to the DCON:

1) The real-time control platform reads in the PMU data and sends a commanded power signal, encoded as a ±10 V analog signal, to the watchdog circuit. This platform is based on the National Instruments PXIe-8135 real-time target.
2) The Windows server provides the graphical user interface, logs relevant data, and performs asynchronous supervisory functions.
3) The watchdog module is a custom-made circuit that monitors the rest of the controller equipment and features an industrial emergency stop safety module.

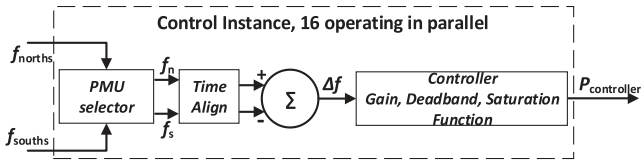

Fig. 4. Block diagram of one of the sixteen control instances operating in parallel from Fig. 3.

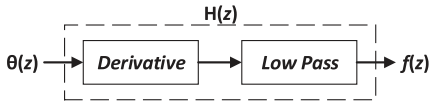

Fig. 5. Block diagram of derivative filter, $H(z)$ from Fig. 3. Further explained in Section III.

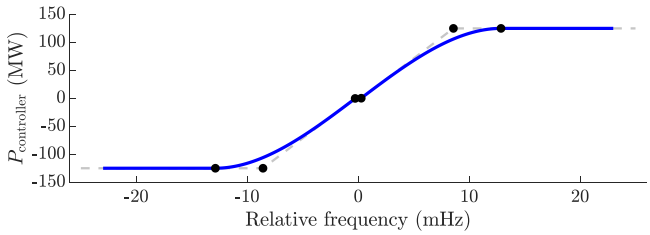

Fig. 6. The gain, deadband, saturation function $K(\Delta f)$ from Fig. 4.

Figs. 3–6 provide additional detail for select elements of the control system. Fig. 3 depicts the real-time controller block from Fig. 2 in detail. The control system employs measurements from four PMUs in the north and four PMUs in the south. This allows for 16 control instances to operate in parallel for redundancy and diversity. The control instances are prioritized based on years of testing to determine the best PMU pairs for feedback control. Whenever the control instance in use experiences an issue, the controller seamlessly transfers to the next highest priority control instance through a bumpless transfer. If all 16 control instances are disabled, the entire control system disarms through a bumpless transfer. The bumpless transfer is utilized in all system state transitions as to never inject any step functions into the system. Any particular control instance is observed in the block diagram in Fig. 4. $H(z)$ is shown in Fig. 5 and further explained in Section III. Fig. 6 depicts the gain, deadband, and saturation function. The deadband in Fig. 6, allows for reduced noise on the PDCI power flow when the system is in steady state conditions.

At the start of the project, it was determined the southern feedback measurement should be at the southern end of the PDCI for the best results [1], but significant research and simulation (Sim) analysis has shown that the southern PMU location in Fig. 1 will suffice if a higher gain is used [8]. The southern measurement in Fig. 1 is selected for practical implementation reasons; the controller was constrained to using measurements within the utility territory for logistical and cybersecurity reasons. In addition, the PMU data can travel on a dedicated fiber network, reducing delays and inconsistencies, which is discussed further in Section V. The adequacy of the southern measurement is illustrated in a simulation in Fig. 7. In addition, the reader is referred to [8]. The simulation in Fig. 7,

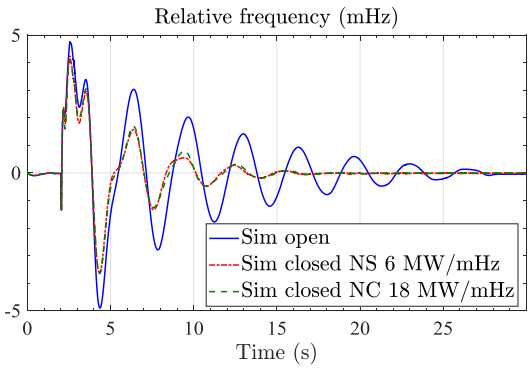

Fig. 7. The relative frequency between the Oregon-Washington border and Oregon-California border during a British Columbia – Alberta separation event. NS feedback is from the Oregon-Washington border to southern California shown with a gain of 6 MW/mHz. NC feedback is from the Oregon-Washington border to the Oregon-California border shown with a gain of 18 MW/mHz.

is of a specific British Columbia – Alberta separation event, using NS (Oregon-Washington border to southern California) feedback verses NC (Oregon-Washington border to Oregon-California border) feedback. These two feedback signals yield almost identical results as long as the gain of the NC case is significantly higher than the gain of the NS case. The limits on the gain are discussed further in Section VI.

III. Filter Design

Although the problem of synthesizing frequency measurements from synchrophasor data is not new [9], it still poses difficult challenges for standards committees, PMU manufacturers, and control system designers. The introduction to C37.118.1-2011 cautions that frequency and rate of change of frequency (ROCOF) "are less reliable measurements, particularly ROCOF, because they are more sensitive to undesirable components in the signal like harmonics, off-nominal components, or noise" [10]. Consistent with this statement, the standard specifies relatively lenient compliance thresholds of 5 mHz for frequency error and 10 mHz/s for ROCOF error. For situational awareness applications, a 5 mHz frequency error may be negligible; however, for the control scheme discussed here, it corresponds to an unacceptable modulation error on the order of 50 MW. Despite these somewhat forgiving specifications, the C37.118.1a-2014 addendum relaxed the criteria further due to compliance difficulties encountered by device manufacturers [11].

A survey of state-of-the art frequency measurement algorithms in the context of real-time control is provided in [12]. Based on the analysis in [12], Hill *et al.* propose a more ambitious maximum frequency error of 1 mHz for control applications. Given the current standards, it cannot be assumed that frequency measurements reported by a particular PMU will meet this more rigorous performance threshold. In order to implement control schemes with such devices, alternative methods of computing frequency are required. In [12], numerical differentiation of the positive sequence voltage angle is shown to nearly satisfy the 1 mHz threshold over the range of nominal frequencies between 59–61 Hz. A 1st-order backward difference derivative with a step size of 1/60 sec and no filter stage is employed.

Here, we improve upon this concept by designing a numerical differentiator that can be viewed as a derivative-filter cascade. In comparison to the method presented in [12], our approach offers lower bias error and better noise rejection.

The sensitivity of frequency measurements to undesirable signal components is a byproduct of the amplitude response of a derivative, which rises by 20 dB per decade. To compensate for this high-frequency sensitivity, we introduce a low-pass filter that aims to attenuate the amplitude response as quickly as possible after 1 Hz. This target marks the upper bound on the frequency of inter-area modes in the WI. The filter was designed to meet the following specifications:

1) phase lag of less than 30° at 0.80 Hz;
2) step response overshoot of less than 10%; and,
3) settling time of less than twice the peak time.

The phase response criterion was selected based on extensive real-world testing of the open-loop transfer function [5]. It aims to preserve an overall phase margin of 60°. The step response criteria ensure that the Q factor of the filter is not excessively high. Recall that the relationship between overshoot and Q is given by

$$\psi = 100e^{-\left(\pi/\sqrt{4Q^2-1}\right)}, \tag{3}$$

where ψ denotes the percent overshoot [13]. The step response and settling time criteria strike a balance between fast initial response and minimal resonance. This precaution mitigates the effect of filter ringing in the critical frequency range between roughly 1–3 Hz where the open-loop phase response transitions through –90°.

A group of candidate filters including both IIR and FIR designs was evaluated. The filter that offered the best compromise between attenuation and the design criteria was a 2nd-order Bessel filter with a –3 dB point near 2 Hz. Recall that Bessel filters are designed in the s-domain and offer a maximally linear phase response, i.e., maximally flat group delay [14]. The bilinear transform was used to convert the transfer function into the z-domain. Let $H_a(s)$ denote the continuous-time transfer function of the filter. The discrete-time representation is produced using the substitution

$$s = \frac{2}{T}\left(\frac{z-1}{z+1}\right). \tag{4}$$

A byproduct of (4) is that the continuous-time transfer function zeros located at $s = \pm j\infty$ are both mapped to $z = -1$. This feature of the conformal mapping was leveraged in the design of the derivative stage. Prewarping was not found to be necessary or beneficial in the overall differentiator design.

The numerical differentiation technique commonly referred to as Tustin's method uses the bilinear transform to approximate an ideal derivative [15], [16]. Evaluating the frequency response of (4) yields

$$H_d\left(e^{j\omega}\right) = \frac{2}{T}\left[\frac{j\sin(\omega)}{1+\cos(\omega)}\right] = \frac{j2}{T}\tan(\omega/2). \tag{5}$$

Thus, the phase response of the Tustin derivative is a constant $\angle H_d(e^{j\omega}) = 90°$ between 0 Hz and the Nyquist frequency. By extension, the phase response of the differentiator precisely matches that of the lowpass filter shifted upward by 90°. The trade-off for this ideal phase response is a pole at $z = -1$. In the absence of a filter stage, this pole causes undesirable high-frequency sensitivity; however, when paired with the lowpass filter described previously, the spurious pole is canceled by one of the filter zeros. To alleviate stability concerns, this pole-zero cancellation is performed analytically during the design procedure. The transfer function of the resulting cascade still has one remaining zero at $z = -1$.

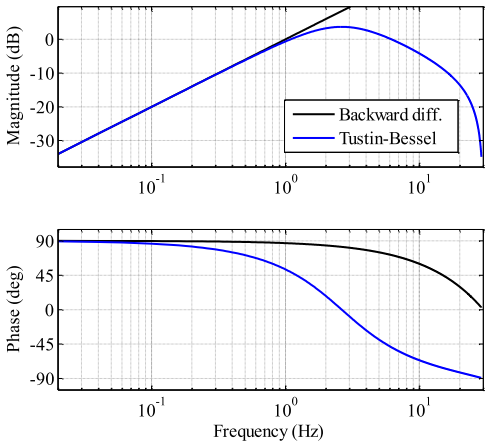

Fig. 8. Numerical differentiator Bode plot.

The input to the numerical differentiator is a positive sequence voltage angle in radians. In practice, precautions need to be taken to account for phase wrapping at the differentiator input. The output is a frequency measurement in Hz, where the numerator coefficients are scaled accordingly. Its transfer function can be expressed as

$$H_f(z) = \frac{b - b\,z^{-2}}{1 - a_1\,z^{-1} + a_2\,z^{-2}}. \tag{6}$$

The coefficients a_1, a_2, and b depend on the PMU reporting rate. For a rate of 60 Hz their values are 1.55725978, 0.61839943, and 0.29192028 respectively. By inspection, we see that (6) has transfer function zeros at $z = 1$ and $z = -1$. It also has a complex pole pair stemming from the lowpass filter. In the time domain, the frequency calculation is given by

$$f(t_k) = b\theta(t_k) - b\theta(t_{k-2}) + a_1 f(t_{k-1}) - a_2 f(t_{k-2}). \tag{7}$$

Fig. 8 compares the frequency response of the final numerical differentiator, comprised of both the derivative and filter stages, with that of a first-order backward difference. As the figure shows, the Tustin-Bessel cascade has much better high-frequency attenuation than the backward difference due to its transfer function zero at $z = -1$. The trade-off for this improved attenuation is an additional 90° of phase lag at the Nyquist frequency.

The open-loop frequency response between the PDCI real power command and the frequency difference between the local and remote points of measurement is shown in Fig. 9. This transfer function estimate was derived from actual system probe testing as described in [5]. The black trace shows the transfer

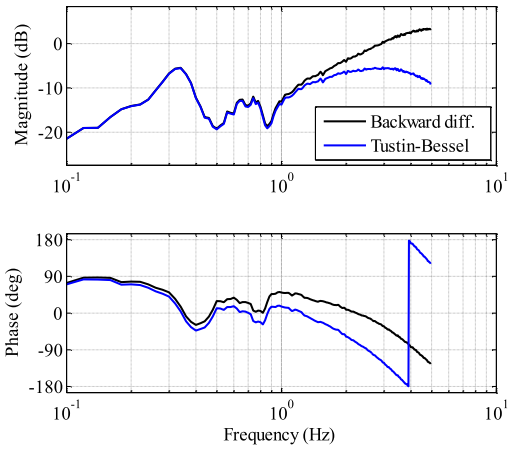

Fig. 9. The uncompensated and compensated open-loop frequency response.

function arising from a 1st-order backward difference derivative with no filtering, and the blue trace arises from the derivative filter cascade in (7) with a 60 Hz reporting rate. As shown in the amplitude response plot, the frequency of the dominant inter-area mode (North-South B) is near 0.35 Hz. Near this resonant peak, the phase response of the blue trace transitions through 0°, which is ideal for damping control. The phase response is near zero for the secondary peaks between 0.6–0.8 Hz (BC and Montana modes) as well. Compared with the backward difference, the cascade in (7) has significantly better high-frequency noise rejection. At 5 Hz, the amplitude response of the cascade is roughly 12 dB lower than that of the backward difference. Likewise, the high-frequency gain of the blue trace is slightly lower than the gain peak near 0.35 Hz, which indicates a reduction in high-frequency gain sensitivity.

IV. Software Design Considerations

When selecting a software development platform, we prioritized support for real-time hardware targets, compatibility with existing substation equipment, and long-term project maintainability. As described later in Section V, the determinism of the control loop is critical in real-time applications. The tight integration between LabVIEW and National Instruments real-time hardware facilitated deterministic control timing. Furthermore, developing in LabVIEW made it possible to leverage elements of existing synchrophasor software applications. Two LabVIEW applications originally developed at the Bonneville Power Administration (BPA) and modified for this project were instrumental in the development of the DCON.

1) Advanced Stream Player (ASP): this program allows for the streaming of historical PMU data in real-time. A simple Windows machine can emulate any number of PMUs. Additional functionality added is the ability to change the time interval between packets, any specified packets can be dropped, and PMU streams can be disabled midstream.
2) StreamReader: This allows the user to read PMU streams in real-time and parse that data, additional code was written to log the data in a format specified by the user.

A third tool was developed and utilized to characterize the network and determine delays in the control loop.

3) PMU Network Characterizer: this program allows for very accurate characterization of the delays in the system. The program reads any number of PMUs specified by an initialization file, as long as the PMU is compliant with the C37.118 standard. The program will characterize the delays for PMUs streaming at different reporting rates in UDP (User Datagram Protocol) or TCP (Transmission Control Protocol). The program timestamps the data as it arrives, and compares it to the timestamp in the PMU data. Multiple tests were completed with this program to verify the system delays were acceptable. This tool was utilized for PMU delay characterization in [17], [18].

The primary LabVIEW code for the controller utilizes parts of both 2 and 3, and was tested with 1. The layout of the controller code has multiple loops operating in parallel with data streaming back and forth between a server and a NI-PXI. The server handles the Graphical User Interface (GUI).

The five loops continuously operating in parallel on the PXI are:

1) The GUI loop; this loop is continuously checking if the user has changed any settings on the GUI.
2) The GPS check loop; this loop continuously checks if the GPS is still active and connected to the controller. This action was found to be computationally expensive, and takes longer than anticipated, therefore it is in its own dedicated loop.
3) The UDP loop; this loop handles the UDP connections and is listening for UDP data streams from the stated IP addresses and ports specified by the initialization file. Once any PMU data packet arrives, it timestamps that data, and places it in a queue.
4) The data parsing/organizing loop; this loop parses the PMU UDP streams and organizes them into queues for each PMU for the main control loop.
5) The main control loop; this loop operates at a constant 60 Hz, i.e., the loop is deterministic at 16.666 ms, 16.667 ms, and 16.666 ms, then repeats.

The main control loop, loop 5, operates as follows.

a) First, the data is pulled off the queue from loop 4 and parsed separately for all 8 PMUs used in this system.
b) The voltage phasors are converted to positive sequence and sent through the derivative filter designed specifically for this project (explained in Section III of this paper). If a data packet does not show up in the 16.666 ms window, the previous data packet is repeated, and the controller is held for a sample, i.e., the derivative filter is not run for a sample. If no packet shows up for 50 ms, the control instances with that PMU are disabled. If two or more data packets show up within one controller loop (16.666 ms), the controller parses all the data packets and runs all the data through the filter in a for-loop, outputting only the last frequency value.
c) Next, in each control instance, the north and south frequencies are time aligned, and the frequency difference is computed.

d) All the data is checked with the supervisory functions, if no flags are on, then the control signal is sent from the PXI to the watchdog circuit; if a supervisory flag is on, the controller outputs a 0 MW signal.
e) In addition, all phasor data, time data, frequencies, relative frequencies, power commands, supervisory flags, controller state, and more information is sent from the PXI to the Windows server to be recorded in a log file.

This completes the main control loop and the software architecture. However, the power command signal still has two more steps until the PDCI acts on that signal. 1) If the watchdog circuit determines the system is operating correctly, i.e., all component heartbeats are alive, and the E-Stop button is not pushed, then all the relays are closed, and the command signal is sent to the PDCI controls. 2) If the PDCI controls have the DCON enabled, the PDCI will act on the commanded power signal by adding the power command to the scheduled power.

Note that initialization of each control instance and the filter is extremely important. If a control instance is disabled due to any supervisory function, even if it is just for one sample, the control instance must go through its entire re-initialization procedure for a safety check, this takes approximately 20 seconds. Although computationally it does not take this long, the controller verifies the data is acceptable for an extended period.

V. Synchrophasor Data Considerations for Operations in Real-Time

This section describes the lessons learned when operating a controller in real-time with synchrophasor data over a wide area network. Excessive delay, data inconsistencies, and data dropouts can significantly degrade a real-time control system [19]; the same is true for the DCON.

A. Inconsistent Data Arrival

Even though PMUs in theory have a constant reporting rate, in practice PMU data packets are not sent to the network at uniformly spaced time intervals. However, when considering a large number of packets, the average reporting rate over a sufficiently large time window is the specified rate. For example, if the reporting rate is 60 samples per second (sps), then theoretically packets should leave the PMU every 16.67 ms; however, actual tests of the PMUs used in this project show that synchrophasor packets leave the PMU at irregular time separations that do not equal 16.67 ms. These tests also show that the average of these time intervals yield 16.67 ms. This behavior is observed in Fig. 10. A PMU may send four packets separated by 16 ms, 9 ms and 25 ms. Note that these time separations can be modified by a wide area network. The takeaway is that a real-time controller operating on PMU data needs to be able to handle inconsistent data arrival.

The main DCON control loop operates at a deterministic 60 Hz. Ideally, a single data packet (per PMU) should arrive within that 60 Hz time window. However, due to the inconsistent data arrival, zero or multiple data packets may arrive in each controller window. This behavior causes the controller output not to be as smooth as it would with uniform data arrival. If

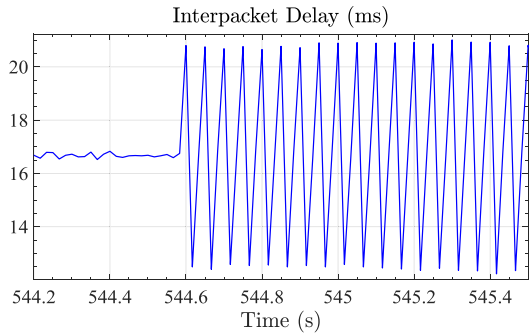

Fig. 10. The time between data packets leaving a PMU. The reporting rate is 60 Hz. Tested by directly connecting a PMU to a network characterizer real-time PXI machine.

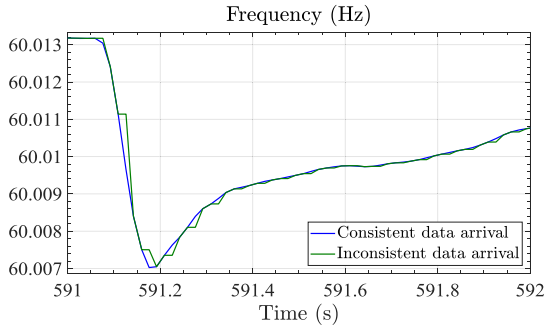

Fig. 11. The power command signal with perfect data arrival (60 Hz, one sample per controller window) vs. inconsistent data arrival (two samples, then zero samples, then two, etc. per controller window).

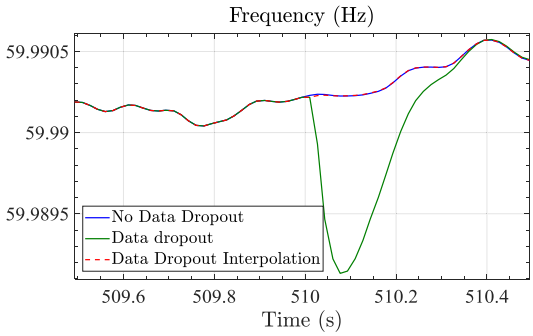

Fig. 12. Effect on the frequency computation during a data dropout.

no data packet arrives within one-time window, the computed frequency is held for one-time window while the controller waits for data; this is shown in Fig. 11. If data does not show up for multiple time windows, the supervisory system would disable the controller instance.

B. Data Dropouts and Faulty Data

In comparison to TCP, UDP offers more efficient group delivery and its throughput it not affected by latency; however, packets can be lost or received out of order with UDP. The DCON treats both situations as data dropouts. If a dropout occurs, it can cause a spike in the frequency calculation in (7) as seen in Fig. 12. To account for this, the DCON checks that successive data frames are separated in time by $1/F_s$, where F_s is the reporting rate in frames per second. If a dropout

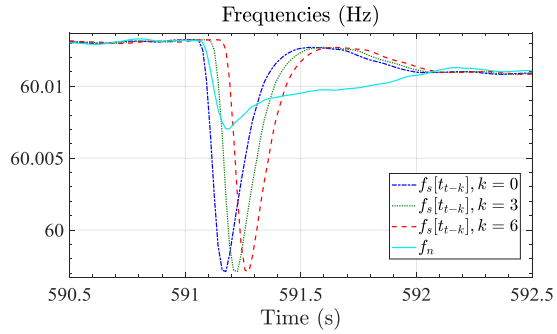

Fig. 13. The frequencies in the north (f_n) and south (f_s) during a generation loss in the south. Frequency in the south is delayed from the frequency in the north by: 0, 3, and 6 samples (0, 50 and 100 ms respectively).

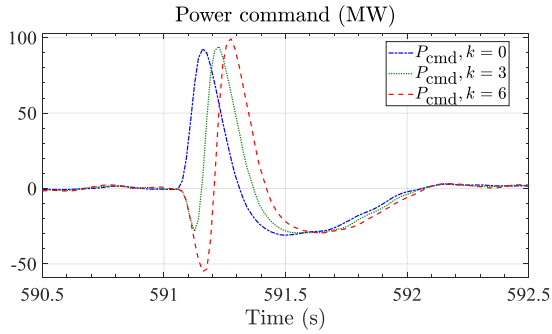

Fig. 14. The power command during a generation loss in the south, when the southern PMU measurement in delayed from the northern PMU measurement by: 0, 3, and 6 samples (0, 50 and 100 ms respectively).

Algorithm 1: Linear Interpolation When The Input Includes Wrapping.

if $\theta_k < 0$ **then**
$\theta_k = 2\pi + \theta_k$
end if
if $\theta_{k-2} < 0$ **then**
$\theta_{k-2} = 2\pi + \theta_{k-2}$
end if
$\hat{\theta}_{k-1} = \frac{\theta_{k-2}+\theta_k}{2}$
if $\hat{\theta}_{k-1} > \pi$ **then**
$\hat{\theta}_{k-1} = \hat{\theta}_{k-1} - 2\pi$
end if

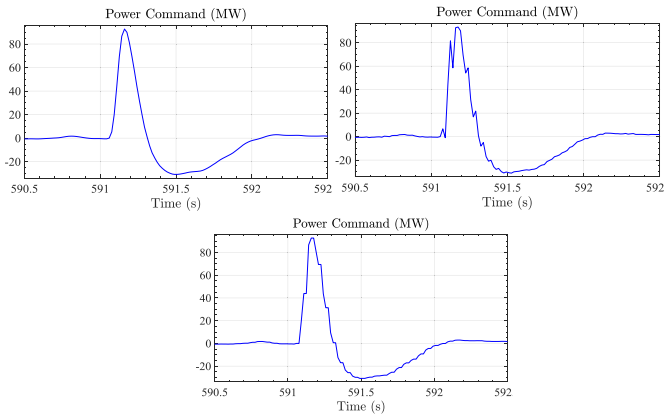

Fig. 15. The power command, (a) top left figure, perfect data arrival, (b) top right figure, inconsistent data arrival without time-alignment, and (c) bottom figure, inconsistent data arrival with time-alignment.

occurs, the controller instance is disabled until the stream recovers. An alternative solution for single packet loss is to use linear interpolation to estimate the missing data. This solution avoids disabling the controller and is shown to be acceptable as depicted in Fig. 12. The linear interpolation method when the input includes wrapping is described in equations in Algorithm 1. The packet dropped is θ_{k-1} and the algorithm needs the packet that comes before it (θ_{k-2}) and after it (θ_k). The estimate for the dropped data is noted as $\hat{\theta}_{k-1} = (\theta_{k-2} + \theta_k)/2$. Data dropouts occur extremely rarely during this project.

Faulty data is handled similarly. This includes C37.118 flags, and values in the data that are out of specific bounds (e.g., delay, voltage angles, voltage magnitudes, frequencies, or derivatives of voltage angles, magnitudes, or frequencies). The supervisory module of the controller has multiple real-time checks that constantly verify the integrity of the data [6]. If at any point the data is deemed invalid, the specific control instance is disabled.

C. Time Alignment

The two signals used in the feedback control must be time-aligned because asymmetric delays between them can have a negative impact on the controller [19]. In (1), f_n and f_s must come from PMU packets with identical GPS timestamps. Time alignment is recommended for the controller to avoid degrading the first swing transient stability of the system. In Fig. 13 and 14, the northern PMU is held constant, and the southern PMU is delayed from northern PMU by 0, 3, and 6 samples (k in Fig. 13 and 14). A generator trip occurs in the south, therefore the frequency in the south drops first, followed by the frequency in the north. With time alignment, $k = 0$, power is initially sent from the north to the south as expected, shown in Fig. 14 with a positive power command. However, if the data from the southern PMU is asymmetrically delayed compared to the northern PMU, the initial power command may be negative, signifying a push of power from the south to the north; this would exacerbate the generation loss in the south. This is shown in Fig. 13 and 14 with asymmetric delays of $k = 3$ and $k = 6$ samples (50 ms and 100 ms respectively). For this reason, f_n and f_s must be time aligned.

D. Inconsistent Data Arrival With Time Alignment

The DCON was designed to be able to handle the circumstances where asymmetric delays occur, and data arrival is inconsistent. Fig. 15a is the ideal case where no asymmetric delay exists, and the data consistently shows up at 60 sps. Fig. 15b is the case where inconsistent packet arrival exists, and asymmetric delay exists with no time-alignment. Fig. 15c presents the result with the same conditions as 15b, but with time-alignment. Fig. 15c is how the controller currently operates under this condition. In short, Fig. 15 illustrates additional need for time-alignment.

TABLE I
THE DCON SYSTEM DELAYS IN MILLISECONDS

Name	Mean	Range	Note
PMU Delay	44	40 – 48	Dependent on PMU settings. Normal distribution.
Communication Delay	16	15 – 40	Heavy tail
Control Processing Delay	11	2 – 17	Normal around 9 ms, but a peak at 16 ms due to control windows when no data arrives (inconsistent data arrival)
Command Delay	11	11	Tests were consistent, fixed 11 ms
Effective Delay	82	69 – 113	Total delay

E. Overall Delays in the Control System

Delay in real-time control can have a detrimental effect on the system. The DCON is acting on modes that occur at 0.2–1.0 Hz. Thus, a small amount of delay is acceptable, but excessive delay may erode stability margins and reduce performance [20]. Experimental results show that the overall delay is on average 82 ms, with a maximum of 113 ms [17]. Table I shows the delays broken up by type.

The 'PMU Delay' is the delay between the timestamp in the data and the time the packet leaves the PMU; this delay primarily comes from the algorithm settings for the PMU. Some of the settings affecting the PMU delay include: the reporting rate, the class of the PMU (either P or M) and/or filtering specifications that some PMU manufacturers use. The 'Communication Delay' is the delay due to the hundreds of miles of ethernet cables, routers, and switches the data travels through. This delay has the most variability. The 'Control Processing Delay' is the time the controller takes to calculate the command signal, and although computation time is 1-2 ms, this delay is dependent on when the data shows up in the deterministic 60 sps control loop. The 'Command Delay' is how long it takes for the PDCI to react to the DCON power command. The 'Effective Delay' is the overall total delay, given as a sum of these delay components.

VI. TEST RESULTS

Before and during development, extensive simulations were performed to determine the impact of the DCON on the dynamics of the WI. Initial simulations were based on the Kundur two area model [21]. This was followed by simulations in the MATLAB based Power Systems Toolbox (PST) [22] on the 122-bus Mini-WECC (Western Electricity Coordinating Council) system, which is a reduced-order model of the WI [23]. Lastly, hundreds of simulations and worst-case scenarios were run on validated full WECC base cases with over 31,000 buses using General Electric's (GE's) Positive Sequence Load Flow (PSLF) software. A custom dynamic model of the DCON was developed in PSLF. Results from some of these simulations are presented in [8].

After the initial implementation, the DCON went through over two years of open-loop testing before closed-loop tests. Open-loop tests are where the controller receives data in real-time, computes the power command, and records it, but no signal is actually sent to the PDCI. Further testing included open-loop probing tests, where a known probing signal is injected into the PDCI and the DCON reacts to these tests. The results from these tests are expanded in [24]. Lastly, closed-loop testing was performed in the Fall of 2016 and Spring of 2017. The initial results from the 2016 tests are presented in [25], [26].

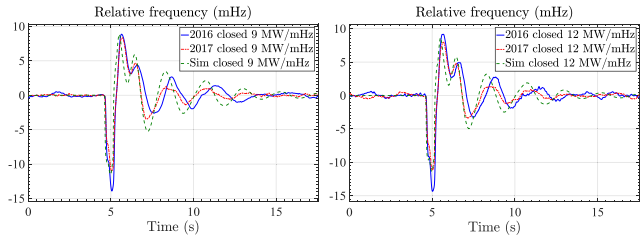

Fig. 16. The relative frequency between the northern and southern measurements during a CJB insertion of 0.5 seconds during actual system tests vs. PSLF simulations; results are shown for (left) a gain of 9 MW/mHz and (right) a gain of 12 MW/mHz.

The highlights of the actual closed-loop tests are the Chief Joseph Brake (CJB) insertions. The CJB is a dynamic braking resistor that adds an almost instantaneous load to the system of approximately 1,400 MW in the center of the state of Washington [27]. This load is connected for 0.5 seconds and immediately causes a large transient event throughout the WI, and the primary mode of interest, the North-South B mode, starts to swing at approximately 0.4 Hz. These tests are coordinated and planned months in advance with multiple utilities in the WECC.

The results shown in Fig. 16 are from the CJB insertion tests and are intended to show how closely correlated the simulations are to the actual system tests. Note that these simulations were performed before the actual tests, the WECC base cases were not modified in any way to produce closer correspondence between the simulated and actual system responses. The simulations use the WECC PSLF light summer 2016 base case. The loading level on the PDCI during the tests vs. the light summer case were comparable.

The main noticeable difference between the actual tests and the simulations is that the simulation case appears to have less inertia in the system and therefore a higher modal frequency of oscillation. Notice in Fig. 16, that the 2017, 12 MW/mHz closed-loop case is relatively flat-lined at the end of the test. This is due to the 0.25 mHz deadband that was included during this test. The deadband reduces the noise on the PDCI while the DCON is enabled.

Figures 17–19 show the relative frequency between the northern measurement and the southern measurement during a 0.5 second CJB insertion event. Fig. 17 is a simulation, and Figs. 18 and 19 are actual system tests where the open loop test is conducted 10 minutes after the closed-loop test. This enables the comparison of the open and closed-loop operation under similar system conditions. The improvement in the damping during closed-loop is significant, illustrated by the damping ratio in Table II. For a given eigenvalue $\lambda_i = \alpha_i + j\omega_i$, the damping ratio ζ_i is defined as

$$\zeta_i = \frac{-\alpha_i}{\sqrt{\alpha_i^2 + \omega_i^2}}. \tag{8}$$

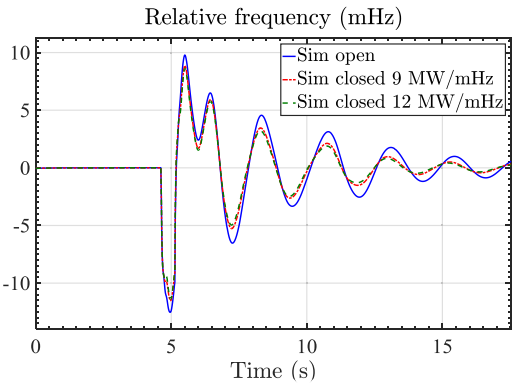

Fig. 17. The relative frequency between the northern measurement and southern measurement during PSLF full WECC simulations (Sim) of a CJB insertion of 0.5 seconds.

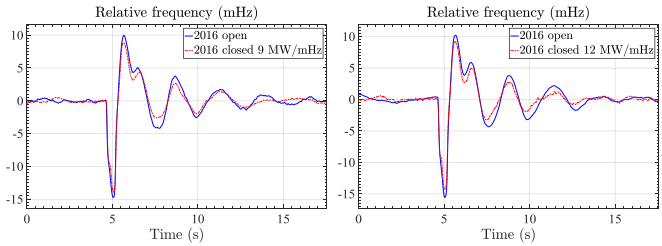

Fig. 18. The relative frequency between the northern measurement and southern measurement during 2016 tests of a CJB insertion of 0.5 seconds.

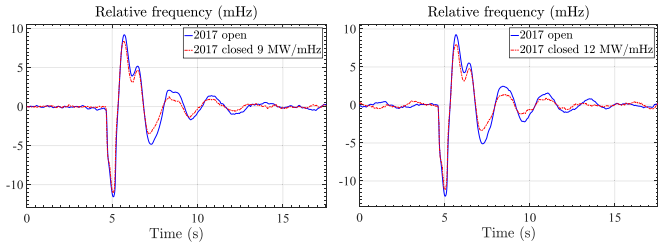

Fig. 19. The relative frequency between the northern measurement and southern measurement during 2017 tests of a CJB insertion of 0.5 seconds.

TABLE II
DAMPING OF THE NORTH-SOUTH B MODE DURING CJB TESTS

CJB Test 9 MW/mHz	Frequency (Hz)		Damping Ratio (%)		Percent Improved
	Open	Closed	Open	Closed	
Simulation	0.425	0.433	7.8	10.3	32.1
2016	0.383	0.361	11.7	16.1	37.6
2017	0.391	0.385	12.8	18.9	32.3

CJB Test 12 MW/mHz	Frequency (Hz)		Damping Ratio (%)		Percent Improved
	Open	Closed	Open	Closed	
Simulation	0.425	0.435	7.8	11.4	46.2
2016	0.424	0.411	12.0	16.0	33.3
2017	0.409	0.420	12.9	16.1	24.8

In Table II, this ratio is expressed as a percentage.

Note that tests were conducted when the system was very stable, and although an increase from 11 to 16% may not seem significant, any substantial improvement in damping ratio is valuable under low-damping conditions. The simulation in Fig. 20 indicates that the improvement is more significant under low damping conditions. The simulation in Fig. 20 is an extreme event in the WI where British Columbia and the U.S. separate

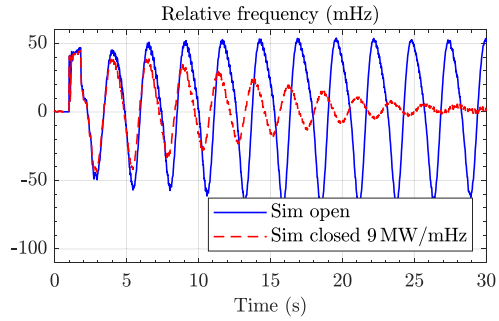

Fig. 20. The relative frequency between the northern measurement and southern measurement during a simulation of a specific British Columbia – U.S. separation event, with and without control.

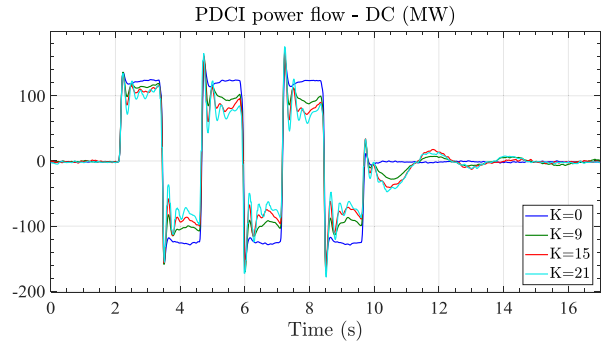

Fig. 21. The dc dynamics with no control and with control of different gains in MW/mHz during 125 MW square wave pulse tests.

in a specific way under dual export conditions, i.e., the northwestern U.S. is exporting power to both Canada and California. The simulation results show an improvement in the damping ratio of the North-South B mode from effectively 0% to 4.1%. To note, Prony analysis is sensitive to the curve fitting parameters (e.g., fit order, time window).

Fig. 21 shows the results from a probing signal insertion into the PDCI of ±125 MW square wave, three cycle pulse at 0.4 Hz with and without control. As shown in the figure, there is a trade-off between the control response and excitation of the PDCI dynamics, i.e., ringing. This interaction influences the maximum feasible controller gain. After testing, a gain of 9–15 MW/mHz was found to limit the PDCI dynamics while allowing significant damping improvement.

VII. CONCLUSION AND FUTURE WORK

This paper comprehensively describes the design and results of the Pacific dc Intertie wide area damping controller. The damping controller significantly improves damping of the North-South B mode of oscillation in the North American Western Interconnection by modulating the power on the Pacific dc Intertie, an 846 mile long ±500 kV dc transmission line that travels from the Oregon-Washington border to Southern California near Los Angeles. This paper describes engineering decisions, simulation analysis, signal processing methods, and control analysis used to design a wide area real-time PMU based feedback control system to help damp inter-area oscillations. The hardware and software architectures for this con-

troller are also described. In addition, this paper depicts how the controller handles multiple PMU data issues in real-time control. Lastly, this paper shows the results from actual system tests with and without the controller enabled; results indicated 4-5% improvement in damping of the North-South B mode without degradation of other modes.

ACKNOWLEDGMENT

The authors gratefully acknowledge the support of the BPA Technology Innovation Office and the U.S. Department of Energy (DOE) Office of Electricity (OE) Transmission Reliability and Energy Storage Programs. At BPA, we would like to thank Mr. Gordon Matthews and Mr. Justin Reel, Project Managers, and Dr. Dmitry Kosterev, Technical Point of Contact. At the DOE-OE Transmission Reliability Program, we would like to thank Mr. Phil Overholt, Program Manager, and at the DOE-OE Energy Storage Program, we would like to thank Dr. Imre Gyuk, Program Manager. This work would not have been possible without their guidance and support. The authors also sincerely appreciate the contributions of BPA engineers Dr. Jisun Kim, Tony Faris, Greg Stults, Dan Goodrich, Jeff Barton, Michael Overeem, Steve Yang, and Mark Yang.

REFERENCES

[1] D. Trudnowski, D. Kosterev, and J. Undrill, "PDCI damping control analysis for the western North American power system," in *Proc. IEEE Power Energy Soc. General Meeting*, Jul. 2013, pp. 1–5.

[2] D. N. Kosterev, C. W. Taylor, and W. A. Mittelstadt, "Model validation for the August 10, 1996 WSCC system outage," *IEEE Trans. Power Syst.*, vol. 14, no. 3, pp. 967–976, Aug. 1999.

[3] C. Lu, X. Wu, J. Wu, P. Li, Y. Han, and L. Li, "Implementations and experiences of wide-area HVDC damping control in China southern power grid," in *Proc. IEEE Power Energy Soc. General Meeting*, Jul. 2012, pp. 1–7.

[4] K. Uhlen, L. Vanfretti, M. M. de Oliveira, A. B. Leirbukt, V. H. Aarstrand, and J. O. Gjerde, "Wide-area power oscillation damper implementation and testing in the Norwegian transmission network," in *Proc. IEEE Power Energy Soc. General Meeting*, Jul. 2012, pp. 1–7.

[5] D. Trudnowski, D. Kosterev, and J. Wold, "Open-loop PDCI probing tests for the western north american power system," in *Proc. IEEE Power Energy Soc. General Meeting*, Jul. 2014, pp. 1–5.

[6] B. Pierre *et al.*, "Supervisory system for a wide area damping controller using PDCI modulation and real-time PMU feedback," in *Proc. IEEE Power Energy Soc. General Meeting*, Jul. 2016, pp. 1–5.

[7] R. Cresap, W. Mittelstadt, D. Scott, and C. Taylor, "Operating experience with modulation of the pacific HVDC intertie," *IEEE Trans. Power App. Syst.*, vol. PAS-97, no. 4, pp. 1053–1059, Jul. 1978.

[8] B. Pierre *et al.*, "Simulation results for the pacific DC intertie wide area damping controller," in *Proc. IEEE Power Energy Soc. General Meeting*, Aug. 2017, pp. 1–5.

[9] A. G. Phadke, J. S. Thorp, and M. G. Adamiak, "A new measurement technique for tracking voltage phasors, local system frequency, and rate of change of frequency," *IEEE Trans. Power App. Syst.*, vol. PAS-102, no. 5, pp. 1025–1038, May 1983.

[10] *IEEE standard for synchrophasor measurements for power systems*, IEEE Standard C37.118.1-2011 (Revision of IEEE Std C37.118-2005), pp. 1–61, Dec. 2011.

[11] *IEEE standard for synchrophasor measurements for power systems – Amendment 1: Modification of selected performance requirements*, IEEE Standard C37.118.1a-2014 (Amendment to IEEE Std C37.118.1-2011), pp. 1–25, Apr. 2014.

[12] B. Hill, D. Trudnowski, and J. Wold, "Frequency estimation for the PDCI inter-area oscillation damping controller," in *Proc. IEEE Power Energy Soc. General Meeting*, Jul. 2016, pp. 1–5.

[13] K. Ogata, *Modern Control Engineering*, 5th ed. Upper Saddle River, NJ, USA: Prentice Hall PTR, 2010.

[14] W. E. Thomson, "Delay networks having maximally flat frequency characteristics," *Proc. IEE - Part III: Radio Commun. Eng.*, vol. 96, no. 44, pp. 487–490, Nov. 1949.

[15] A. Oppenheim and R. W. Schafer, *Discrete-Time Signal Processing*, 3rd Ed. Upper Saddle River, NJ, USA: Prentice-Hall, Inc., 2010.

[16] K. Åström and B. Wittenmark, *Computer-Controlled Systems: Theory and Design*, 2nd Ed. Upper Saddle River, NJ, USA: Prentice-Hall, Inc., 1990.

[17] F. Wilches-Bernal *et al.*, "Time delay definitions and characterization in the pacific DC intertie wide area damping controller," in *Proc. IEEE Power Energy Soc. General Meeting*, Jul. 2017, pp. 1–5.

[18] C. Lackner, F. Wilches-Bernal, B. J. Pierre, and D. A. Schoenwald, "A tool to characterize delays and packet losses in power systems with synchrophasor data," *IEEE Power Energy Technol. Syst. J.*, vol. 5, no. 4, pp. 117–128, Dec. 2018.

[19] F. Wilches-Bernal, B. Pierre, D. Schoenwald, R. Elliott, and D. Trudnowski, "Time synchronization in wide area damping control of power systems," in *Proc. IEEE Probabalistic Methods Appl. Power Syst.*, Jun. 2018, pp. 1–6.

[20] J. Neely *et al.*, "Damping of inter-area oscillations using energy storage," in *Proc. IEEE Power Energy Soc. General Meeting*, Jul. 2013, pp. 1–5.

[21] M. Klein, G. Rogers, and P. Kundur, "A fundamental study of inter-area oscillations in power systems," *IEEE Trans. Power Syst.*, vol. 6, no. 3, pp. 914–921, Aug. 1991.

[22] J. H. Chow and K. W. Cheung, "A toolbox for power system dynamics and control engineering education and research," *IEEE Trans. Power Syst.*, vol. 7, no. 4, pp. 1559–1564, Nov. 1992.

[23] D. Trudnowski and J. Undrill, "The MinniWECC System Model," in "Oscillation damping controls," BPA, Portland, OR, United States, contract 37508, year 1 report, Sep. 2008.

[24] B. Pierre *et al.*, "Open-loop testing results for the pacific DC intertie wide area damping controller," in *Proc. IEEE Power Energy Soc. Power Tech*, Jun. 2017, pp. 1–6.

[25] D. Trudnowski *et al.*, "Initial closed-loop testing results for the pacific DC intertie wide area damping controller," in *Proc. IEEE Power Energy Soc. General Meeting*, Aug. 2017, pp. 1–5.

[26] D. A. Schoenwald, B. J. Pierre, F. Wilches-Bernal, and D. J. Trudnowski, "Design and implementation of a wide-area damping controller using high voltage DC modulation and synchrophasor feedback," in *Proc. Int. Fed. Autom. Control 20th World Congr.*, Jul. 2017, pp. 1–6.

[27] M. Shelton, W. Mittelstadt, P. Winkelman, and W. Bellerby, "Bonneville power administration 1400-MW braking resistor," *IEEE Trans. Power App. Syst.*, vol. 94, no. 2, pp. 602–611, Mar. 1975.

Brian J. Pierre (S'09–M'15) received the B.S. degree in electrical engineering from Boise State University, Boise, ID, USA and the M.S. and Ph.D. degrees in electrical engineering, focused on electric power systems from Arizona State University, Tempe, AZ, USA. He is presently a Senior Member of Technical Staff in the Power Systems Research Department at Sandia National Laboratories, Albuquerque, NM, USA. His research interests and expertise include power system modeling, power system controls, renewable energy integration, power system resilience, and power system optimization. In 2017, for the project described in this paper, all the authors received an R&D 100 Award.

Felipe Wilches-Bernal (S'12–M'16) received the M.S. degree in control systems and signal processing from the Université Paris-Sud XI, Orsay, France and the Ph.D. degree in electrical engineering from Rensselaer Polytechnic Institute, Troy, NY, USA. He joined the Electric Power Systems Research Department at Sandia National Laboratories, Albuquerque, NM, USA in 2015 where he currently works as a Senior Member of Technical Staff. His research experience and interests include power system stability and control, renewable energy and smart grid technologies, and signal processing and control techniques applied to power systems.

David A. Schoenwald (S'84–M'92–SM'02) received the Ph.D. degree in electrical engineering from The Ohio State University, Columbus, OH, USA. He was with the Instrumentation and Controls Division at Oak Ridge National Laboratory, Oak Ridge, TN, USA. He is a Principal Member of Technical Staff in the Electric Power Systems Research Department at Sandia National Laboratories, Albuquerque, NM, USA. In his current work, Dr. Schoenwald focuses on control system design for damping inter-area power system oscillations. His interests also include development of performance standards for grid-scale energy storage.

Ryan T. Elliott (S'11–M'12) received the M.S.E.E. degree from the University of Washington, Seattle, WA, USA, in 2012. He is working towards the Ph.D. degree with the Department of Electrical and Computer Engineering, University of Washington. His research focuses on renewable energy integration, wide-area measurement systems, and power system operation and control. He is also a contributor to the Electric Power Systems Research Department at Sandia National Laboratories, Albuquerque, NM, USA, where he was a member of technical staff from 2012–2015. During his tenure at Sandia, he served on the WECC Renewable Energy Modeling Task Force, leading the development of the WECC model validation guideline for central station PV plants.

Daniel J. Trudnowski (M'91–SM'99–F'09) received the B.S. degree in engineering science from Montana Tech, Butte, MT, USA, in 1986, and the M.S. and Ph.D. degrees in electrical engineering from Montana State University, Bozeman, MT, USA in 1988 and 1991, respectively. From 1991 to 1995, he was with Battelle, Pacific Northwest National Laboratory, Richland, WA, USA where he was a Senior Research Engineer. In 1995, he joined Montana Tech, Butte, MT, USA, where he is currently the Dean of the School of Mines and Engineering, and Professor in electrical engineering research activities. Over the past 25 years, he has primarily focused on problems related to power system dynamics and controls. Dr. Trudnowski is a member of the IEEE Power System and Control System Societies and is a Registered Professional Engineer in the State of Montana.

Raymond H. Byrne (S'86–M'89–SM'07–F'17) received the B.S. degree in electrical engineering from the University of Virginia, the M.S. degree in electrical engineering from the University of Colorado, Denver, CO, USA, the M.S. degree in financial mathematics (financial engineering) from The University of Chicago, Chicago, IL, USA, and the Ph.D. degree in electrical engineering from The University of New Mexico, Albuquerque, NM, USA. He is currently the Manager of the Electric Power Systems Research Department at Sandia National Laboratories, Albuquerque, NM, USA, where he has been employed since 1989. He also serves as the Team Lead of the Equitable Regulatory Environment thrust area of the Sandia energy storage program. His awards include Time Magazine Invention of the Year in Robotics in 2001 and the Prize Paper Award at the 2016 IEEE Power and Energy Society General Meeting for a paper on "Maximizing revenue from energy storage in grid applications". Dr. Byrne is a member of Tau Beta Pi, Eta Kappa Nu, and Sigma Xi. He was elevated to IEEE Fellow for contributions to miniature robotics andgrid integration of energy storage in 2017.

Jason C. Neely (M'05–SM'16) received his B.S. and M.S. degrees in electrical engineering from the University of Missouri-Rolla, Rolla, MO, USA, in 1999 and 2001 respectively. He then worked at Sandia National Laboratories, Albuquerque, NM, USA, in the Intelligent Systems and Robotics Center, focusing on circuits and embedded controllers for power and control of autonomous and remotely-operated systems. In 2010, he earned his Ph.D. degree in electrical and computer engineering from Purdue University, West Lafayette, IN, USA, with a focus in optimal controls for power electronic converters and systems. Dr. Neely is currently a Principal Member of Technical Staff at Sandia National Laboratories, working on the integration of power electronics for grid and national security applications.